Behaviour of dissimilar weld joint of steels FB2 and F during long-term creep test

J Kasl[1], D Jandová[1] and V Kanta [1]

Výzkumný a zkušební ústav Plzeň s.r.o., Tylova1581/46, 301 00 Plzeň, the Czech Republic

E-mail: kasl@vzuplzen.cz

Abstract. Creep test to the rupture of both the dissimilar weld joint made of FB2 and F martensitic steels and the base materials was carried out at temperatures ranging from 550 °C to 650 °C in the stress range from 70 to 220 MPa. Creep rupture strengths of the weld joint and the base materials were evaluated using Larson-Miller parameter. Assessment of microstructure development and changes of hardness was correlated with the creep strength. Critical zones of creep damage were determined. At lower temperatures and higher stresses the weld joint ruptured in the base material of F steel unaffected by welding, while at higher temperatures and lower stresses rupture occurred in the intercritical heated and fine-grained parts of heat affected zone of steel F. During creep at temperatures above 575 °C Laves phase precipitated in all parts of the weld joint and especially in the heat affected zones. Coarse Laves phase particles and their clusters with chromium carbides served as nucleation centres for cavities. As the fine grained heat affected zone of F steel was the softest part of the weld joint, many cavities originated and initiated causing failure of samples.

1 Introduction

There are many ongoing discussions dealing with the benefits of nuclear and steam power plants and renewable power sources in terms of economy, the environment and safety. Fossil fuel power plants cater for more than 60 % of the world's production of electricity and it is expected that they will be the most important sources of electricity in the near future in spite of the increasing role of renewable sources.

The continuous trend towards more economic electricity production together with reduced environmental pollution can be sustained by improving the thermal efficiency of power generation plants. One way to increase the efficiency of fossil power plants is to increase the temperature and pressure of the steam which finally results in the need for improved materials for the boiler and turbine design.

The class of the 9-12% Cr steels is currently used for critical components in plants operating at ultra-supercritical conditions of steam. These steels show high long-term creep strength and oxidation resistance in steam, along with ease of welding and fabrication of large forgings, castings and pipe sections. Both F and FB2 steels were developed in the under the European COST programmes [1] for the production of large scale forgings for applications with creep conditions at temperatures up to 600 °C and 620 °C respectively.

The rotor is one of the most important components of steam turbines. Large rotors for turbines of high power can be produced in the form of a solid forging or as a component welded of several

parts. The welded rotors have the following advantages in comparison with solid-forged ones: application of different materials with optimal properties for different parts of a rotor at given operating conditions (properties of the rotor are gradually changed from the low pressure to the high pressure part), reduction in weight of welded parts, which can be forged more precisely than large ones, higher metallurgical accuracy, reduced heat load and faster start-up.
Doosan Škoda Power Ltd. has established a station for vertical welding of heavy components up to 135 tonnes. It, among other parts, enables automated welding of turbine rotors for single-casing turbines intended for high-temperature steam input (600 °C) as well as for low-pressure components of the highest output rating turbines. A trial dissimilar weld joint of steels COST F and COST FB2 was prepared in the conditions used for industrial welded rotor production. Specimens were machined, creep tested and analysed at the Research Testing Institute in Plzeň, Ltd. This paper deals with the results of these analyses.

2 Experiments

2.1 Materials and welding process

Dissimilar weld joints were prepared from forgings of two rings (external diameter of 600 mm and thickness of 200 mm) made of steels type COST FB 2 ((X13CrMoCoVNbN9-1-1) – the base material 1 (BM 1) and COST F (X14CrMoVNbN10-1) – the base material 2 (BM 2). Producer of both the forgings was SAARSCHMIEDE Gmbh Freiformschmiede according to the specification of Doosan Skoda Power Ltd. The quality heat treatment of forgings was 1070°C/6,5h + 570°C/12,5h + 710°C/24h and 1050°C/6h + 1100°C/6h + 570/12,5h + 720/24h for the base material 1 and the base material 2 respectively. Two filler materials were tested, namely Thermanit MTS 3 (W-CrMo91) and PSM Thermanit MTS 616 (W-ZCrMoWVNb). Welds were carried out using automated welding method 141+111 (TIG HOT WIRE) into narrow gap with internal protection by argon. The thickness of welded walls was 120 mm. Three post-weld heat treatments (PWHT) processes were applied to the weldments. On the basis of evaluation of mechanical properties, hardness and microstructure observation, the weld joint with the weld metal of THERMATIT MTS 616 and the second PWHT were chosen as the most promising variant for rotor production. For inspections of welded zones after post-heating treatments, the ultrasonic testing TOFD method was used as well as standard NDT surface inspection. The chemical compositions of the base materials COST F and COST FB2 and the filler metal used are given in Table 1.

Table 1. Chemical composition of the base materials and filler metal [w-%].

Mater.	C	Mn	Si	Cr	Ni	Mo	V	Co	W	Nb	N	B
BM1	0.13	0.34	0.08	9.6	0.17	1.48	0.2	1.32	-	0.016	0.016	0.0079
BM2	0.11	0.56	0.06	10.36	0.64	1.46	0.2	-	-	0.059	0.016	-
WM	0.11	0.42	0.3	8.87	0.57	0.56	0.18	0.15	1.49	0.051	0.018	0.0036

2.2 Sample preparation and used methods

Smooth cross-weld specimens with a length of 92 mm and a diameter of 8 mm were fabricated from the weld joint as well as from both the base materials. Long-time creep tests to the rupture of these specimens were carried out. Fracture surfaces of ruptured samples were observed using scanning electron microscope (SEM). Then specimens were cut along their longitudinal axis. Macrostructure was revealed using Villela-Bain´s reagent and location of fracture in the weldment was specified. Hardness measurement along the specimen axis was performed. Microstructure of longitudinal sections was observed using light microscopy (LM) and scanning electron microscopy (SEM). The substructure was evaluated in a transmission electron microscope (TEM) from carbon extraction replicas and thin foils. Quantitative evaluation of precipitates was performed using SEM micrographs and the image analysis program NIS–Elements.

3 Results

3.1 Mechanical properties

Integrity and mechanical properties of weld joint have been evaluated according to the welding standards EN 288-2,3. All results were satisfactory according to demands of rotor producer.

3.2 Creep tests

The creep rupture testing was carried out in air at temperatures ranging from 550 °C to 650 °C and stresses from 70 MPa to 220 MPa. The longest time to the rupture of samples so far is about 11,000 hours. A list of specimens investigated is given in Table 2. Results of creep tests as a dependence of applied stress on time to rupture are shown in Fig. 1. Obtained creep data were evaluated using the Larson-Miller parametric (LMP) equation (1):

$$P = T * (C + log\tau) \quad (1)$$

where T represents temperature given in degree Kelvin, C is a specific constant for a given material (equal 36) and τ means time to rupture in hours. Results of creep strength of the weld joint compared with the creep rupture strength data of original COST F steel [2] and creep results of the base material BM2 are graphically represented in Fig. 1.

Table 2. List of creep tested samples and some results (time to rupture in h, fracture position and LRF and SRF factors).

		Weld join		BM 2 - COST F	BM 1 - COST FB2			
Temp. [°C]	Stress [MPa]	Duration [h]	Location of fracture surface	Duration [h]	Duration [h]	Note	SRF	LRF
550	180	52 566	IC/FG HAZ F				0.97	0.45
550	200	17 626	F				0.98	0.83
575	130	39 063	IC/FG HAZ F				0.88	0.23
575	150	15 746	IC/FG HAZ F				0.98	0.37
575	200	1 354	F	799	6 406		1.03	1.59
575	220	653	F	465	3 009		1.02	2.67
600	90	21 294	FG/CG HAZ F				0.79	0.22
600	100	11 288	FG HAZ F				0.84	0.28
600	120	11 264	FG HAZ F	12 365	(41 311)	in progress	0.84	0.40
600	140	3 656	IC/FG HAZ F	9 888	(22 649)	in progress	0.99	0.56
600	160	2 712	F				1.02	0.93
600	180	577	F	586	13 626		1.09	1.65
625	80	7 137	FG/CG HAZ F	26 133	(35 056)	in progress	0.81	0.28
625	90	4 736	FG HAZ F				0.82	0.43
625	100	1 939	FG HAZ F	11 621	(23 249)	in progress	0.88	0.53
625	120	896	FG HAZ F				0.99	0.71
625	140	815	IC/FG HAZ F	372	4 985		1.01	1.04
650	70	3 552	FG/CG HAZ F	11 681			0.86	0.20
650	80	2 741	FG HAZ F (other crack)				0.89	0.52
650	100	343	FG HAZ F	394	1 410		0.94	0.98

The creep strengths of samples tested at 550°C, 575 °C, and 650 °C are in the permitted scatter band ± 20 % of the creep strength of the base material COST F. The creep strengths of the samples tested at 600 °C and 625 °C fall into the scatter band 20 % of the creep strength of the base material COST F with the exception of the sample tested at the lowest stresses, which are below this scatter band.

In order to compare welding influence on creep strength two parameters were evaluated, namely the stress reduction factor SRF

$$SRF = (\sigma_W/\sigma_{BM})_{T,t} \quad (2)$$

where σ_W and σ_{BM} are stresses needed for a given time to rupture τ at a given temperature T of the welded and non-welded material; and the life time reduction factor LRF

$$LRF = (t_W/t_{BM})_{T,\sigma} \quad (3)$$

where τ_W and τ_{BM} are the time to rupture needed for a given stress σ at a given temperature T of the welded and non-welded material BM2. Both evaluated SRF and LRF factors are shown in table 2.

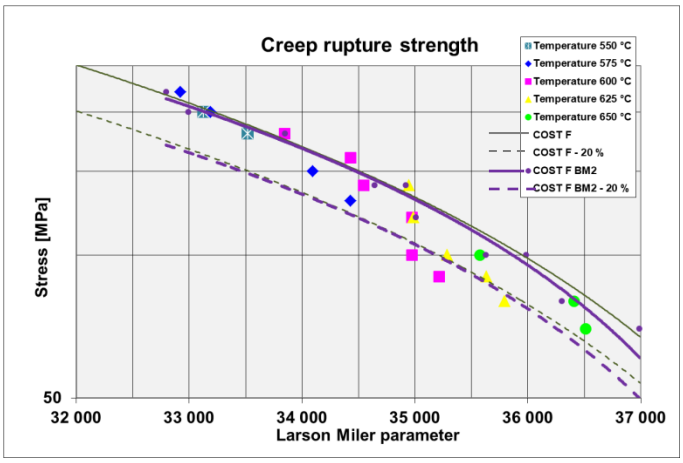

Figure 1. Creep rupture strength vs. LMP.

3.3 Fractographic analysis

Fractographic analysis of broken samples was performed. Firstly, it should eliminate the influence of possible defects formed during the welding process on creep results and secondly, it should find the growth mechanisms of cracks. The samples tested at lower temperatures and higher stresses failed in the base material of steel COST F unaffected by welding while those tested at higher temperatures and lower stresses ruptured in the grain refined part (FG) or in the intercritically reheated part (IC) of the heat-affected zone (HAZ) of the base material of steel COST F. Fractures in the BM occurred after short durations of creep tests. They were transcrystalline ductile with considerable macroplastic deformation (elongation about 18 %) and with the dimple morphology of the fracture surface. Fractures in the HAZ occurred by transgranular creep rupture. Elongations of these specimens were usually a few percent (figure 2).

Fractographic analysis and observation of longitudinal sections of the ruptured crept samples showed that locations of fractures depended on the creep conditions. The proper positions of fracture change from IC part of the HAZ to boundary between FG and coarse grained (CG) parts of the HAZ with increasing temperature and decreasing stress (table 2).

3.4 Hardness profiles measurement

Creep exposures resulted in the samples softening, which was evident from the Vickers Hardness profiles across the weld joint. The hardness of the weld metal (WM) slightly decreased, from 280 HV10 of the virgin specimen to 260 HV10 after creep at 650°C/70 MPa/3552 h. Decrease in the base materials was more significant, from 240 HV10 of the base materials to 213 HV10 of BM1 after creep at 650°C/70 MPa/3552 h and to 204 HV10 of BM2 after creep at 625°C/120 MPa/896 h. No important decrease was found in the HAZ of BM1, while a decrease from 220 to 185 HV10 occurred in the HAZ of BM2. Hardness profiles of the virgin specimen and crept specimens are shown in figure 3.

Figure 2. Macrographs of specimens creep tested at conditions: a) 575°C/200MPa/1345h and b) 600°C/80MPa/21294h.

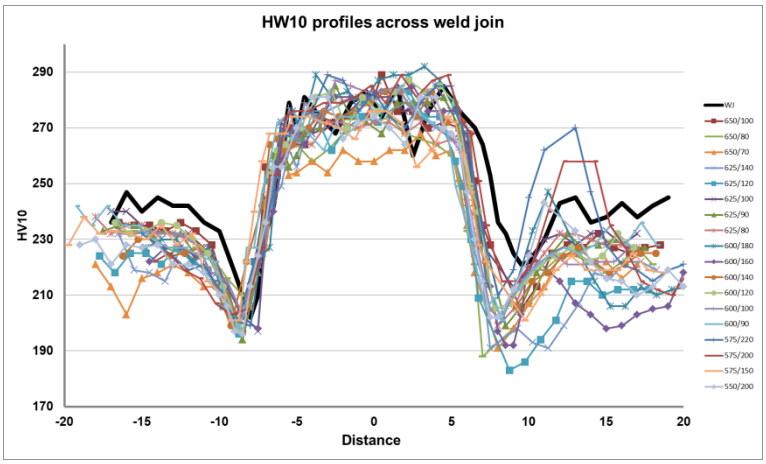

Figure 3. Vickers hardness profiles of specimens creep tested compared with not tested one (WJ).

3.5 Microstructure evaluation

The width of heat affected zones ranges from 2.5 to 3.0 mm on both sides of the weldment. Sizes of prior-austenitic grains are different in various parts of the weldment. Grain size of steel COST FB2 (about 90 μm) is significantly larger in comparison with steel COST F (about 21 μm). Average grain sizes of both the HAZs and the weld metal are comparable with grain sizes of steel F (about 20 μm). Grain sizes of coarse–grained parts of HAZs are only slightly larger compared with fine–grained parts of HAZs; from 28 to 17 μm and from 38 to 14 μm for HAZ FB2 and HAZ F respectively. Also average grain sizes in both the cast and heated parts of the weld metal are similar although the form of the grains is different.

Microstructure of the BM1 consisted of heavy tempered martensite with a small amount of δ-ferrite. Coarser prior austenitic grains contain packets of martensitic laths; some of them are subdivided into subgrains. The main contributor in suppressing the recovery of martensitic structure was a dispersion of $M_{23}C_6$ and fine vanadium carbonitride particles. However non-uniform distribution of fine vanadium carbonitrides was observed within laths. Dislocation density was about $4 \cdot 10^{14}$ m^{-2}. The WM also consisted of tempered martensite containing islands of δ-ferrite. Coarser particles of carbides rich in W, Mo, Cr, V together with some rare particles of Laves phase were observed in the WM, which is alloyed with tungsten. Dislocation density was about $5 \cdot 10^{14}$ m^{-2}. The main precipitate was $M_{23}C_6$, fine particles of V(N,C) were also present. The BM2 is fine-grained. Similar average grain size was also observed in their HAZ with only slightly higher average size in coarse-grained region. Martensitic lath structure is conserved here and laths contain subgrains only locally. On the other hand prior austenitic grains are subdivided into small equiaxed subgrains or new grains in the fine-grained region. Fine vanadium/niobium MX carbonitrides were spread within ferrite laths more often in the BM2 and also in the weld metal than in the BM1. In contrast, the density of chromium carbides was higher in the BM1 than in other parts of the weldment. Dislocation density in the BM2 was the highest, about $6 \cdot 10^{14}$ m^{-2}.

After creep testing in a temperature range from 600 to 650 °C and a stress range from 70 up to 150 MPa, cavities were detected in all parts of the weld joint. Cavitation failure in the heat affected zones on both sides of the weld joint was evident. More cavities always occurred in the HAZ of steel F and their coalescence resulted in fracture.

Some differences were found in individual zones of the weld joint, which caused premature fracture in specific zones depending on the conditions of the creep test. All structures observed corresponded to heavy tempered martensite with a high density of secondary phases. Significant differences were found in the structure recovery in the base materials, their heat affected zones and the weld metal. Small differences were found in the size and distribution of the precipitates.

Concerning the size and distribution of two of the most important secondary phases – $M_{23}C_6$ and MX particles, no important changes were found after creep tests. Intensive precipitation of Laves phase occurs in the temperature range from 600 to 625 °C. Precipitation of Laves phase occurred across the whole of the weld joint, however it was especially concentrated in the heat affected zones and the weld metal. Under the highest stress the controlling mechanism of the fracture was slip of dislocations. The grain boundaries in the HAZ pinned with $M_{23}C_6$ carbides and Laves phase particles effectively hindered the dislocation movement, and fracture occurred in BM2. Diffusion, grain-boundary sliding and dislocation climbing became more important with decreasing stress. At rather lower stresses dislocation slip and grain boundary sliding were probably equivalent processes of creep deformation. Soft small grains along previous austenite grain boundaries were deformed by slip and plastic deformation was accommodated by grain boundary sliding. In sites where soft grains were adjacent to the relatively hard lath-like base material, cavities originated as well as at grain boundaries with numerous coarse carbides.

Fractures occurred in IC HAZ, where the surface of the grain boundaries was larger than in other zones of the joint. A further decrease in stress resulted in fractures in the FG HAZ – a zone consisting of a recovered structure with soft grains separated by high angle boundaries and well developed subgrains. The slip of such grains could activate slip and consequent sliding of boundaries with jogs and coarse precipitates could originate cavities. Creep at the lowest stresses resulted in fracturing near the CG HAZ. Before creep testing, small recrystallized grains surrounded with lath-like structures with very high dislocation density occurred in this region. At high temperatures and low stresses, recovery in the regions close to the prior austenite grain boundaries played an important role. Cavities originated in these well-recovered grains, and cracks were created.

4 Conclusions

Creep testing of weld joint of COST F and COST FB2 steels designed for production rotors for fossil fuel power plants revealed sufficient creep strength, only slightly lower than that of the weaker base material steel COST F for temperatures up to 575 °C.

During creep testing the highest decrease of the hardness occurred in the intercritically reheated or in the over-tempered parts of HAZ of steel COST F where samples failed. The critical zone of the weld joint in terms of creep failure was the heat affected zone of steel COST F.

Precipitation of Laves phase and structure recovery during creep exposures at temperatures in a range from 550 to 650 °C were the main reasons for the failure. Different stages of the structure recovery and precipitation were observed in the heat affected zones in relation to the conditions of creep exposure. Consequently, contribution of individual processes taking place during creep at high temperatures – dislocation slip, climbing, grain boundary slipping and diffusion, were different in CG, FG and IC HAZ and caused a systematic shift of fracture from COST F steel to its CG HAZ. Softening of the matrix and coarsening of secondary phases as a result of Laves phase precipitation caused predominantly cavitation failure in the heat affected zone and crack propagation. Precipitation of Laves phase seems to be most significant at a temperature of 600 °C.

Acknowledgements

This work was supported by Grant TE01020118 from the Technology Agency of the Czech Republic.

References

[1] Kern T-U, Mayer K H, Donth B, Zeiler G and DiGianfrancesco A 2010 The European efforts in development of new high temperature rotor materials – COST536, in: Lecomte-Beckers J, Contrepois Q, Beck T and Kuhn B (Eds.), Materials for Advanced Power Engineering (Forschungzentrum Jülich GmbH, Jülich) pp 29–38

[2] Results of creep test of COST 522 programme; a set of internal documents available for participants of programme